Atmos. Chem. Phys., 13, 9731–9744, 2013
www.atmos-chem-phys.net/13/9731/2013/
doi:10.5194/acp-13-9731-2013

Atmospheric Chemistry and Physics Open Access

Naphthalene SOA: redox activity and naphthoquinone gas–particle partitioning

R. D. McWhinney, S. Zhou, and J. P. D. Abbatt

Department of Chemistry, University of Toronto, Toronto, ON, Canada

Correspondence to: J. P. D. Abbatt (jabbatt@chem.utoronto.ca)

Received: 20 March 2013 – Published in Atmos. Chem. Phys. Discuss.: 5 April 2013
Revised: 26 July 2013 – Accepted: 12 August 2013 – Published: 2 October 2013

Abstract. Chamber secondary organic aerosol (SOA) from low-NO_x photooxidation of naphthalene by hydroxyl radical was examined with respect to its redox cycling behaviour using the dithiothreitol (DTT) assay. Naphthalene SOA was highly redox-active, consuming DTT at an average rate of 118 ± 14 pmol per minute per µg of SOA material. Measured particle-phase masses of the major previously identified redox active products, 1,2- and 1,4-naphthoquinone, accounted for only 21 ± 3 % of the observed redox cycling activity. The redox-active 5-hydroxy-1,4-naphthoquinone was identified as a new minor product of naphthalene oxidation, and including this species in redox activity predictions increased the predicted DTT reactivity to 30 ± 5 % of observations. These results suggest that there are substantial unidentified redox-active SOA constituents beyond the small quinones that may be important toxic components of these particles. A gas-to-SOA particle partitioning coefficient was calculated to be $(7.0 \pm 2.5) \times 10^{-4}$ m^3 µg^{-1} for 1,4-naphthoquinone at 25 °C. This value suggests that under typical warm conditions, 1,4-naphthoquinone is unlikely to contribute strongly to redox behaviour of ambient particles, although further work is needed to determine the potential impact under conditions such as low temperatures where partitioning to the particle is more favourable. Also, higher order oxidation products that likely account for a substantial fraction of the redox cycling capability of the naphthalene SOA are likely to partition much more strongly to the particle phase.

1 Introduction

Exposure to particulate matter (PM) is known to be a concern to human health. Oxidative stress induction is believed to be a major toxicological mechanism of inhaled particles. For example, reactive oxygen species have been observed to quickly rise in the lungs and hearts of rats after inhalation of ambient particles (Gurgueira et al., 2002), and oxidative stress mechanisms have been implicated in playing a role in asthma (Gurgueira et al., 2002; Li et al., 2003a) and other respiratory diseases (Li et al., 2008).

Inducing oxidative stress can involve either producing an excess of oxidants or depleting antioxidants within a cell. One chemical mechanism for inducing oxidative stress is through redox cycling reactions, where efficient redox cycling catalysts can accept electrons from electron-rich reducing agents; subsequently, the electrons are transferred to molecular oxygen to generate superoxide, allowing the cycle to repeat. This process has the potential to both deplete antioxidant species in the cell and generate reactive oxygen species, contributing to induction of oxidative stress. Redox cycling capacity can be measured using an acellular technique known as the dithiothreitol (DTT) assay (Kumagai et al., 2002). In the assay, a buffered aqueous extract of a PM sample is mixed with DTT, which contains two electron-rich thiol groups. The catalytic capacity of DTT to transfer these electrons to molecular oxygen can be observed by measuring the DTT rate of decay, which has been correlated to oxidative stress markers in cellular systems (Li et al., 2003b; Koike and Kobayashi, 2006). Constituents of PM that have been shown as active redox cycling catalysts include black carbon from diesel particles (Shinyashiki et al., 2009),

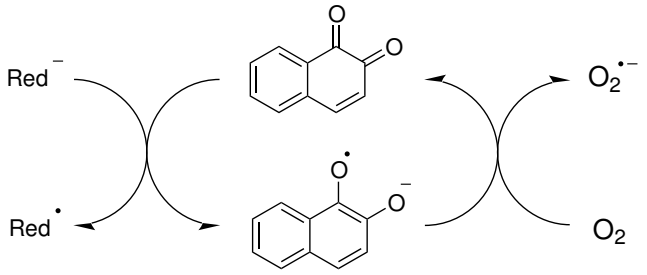

Fig. 1. A general redox cycle for 1,2-naphthoquinone. A generic reducing agent (Red) transfers a single election to 1,2-naphthoquinone to generate the semiquinone radical. The quinone is regenerated when the electron is transferred to oxygen, generating superoxide.

transition metals (Netto and Stadtman, 1996; Charrier and Anastasio, 2012), humic-like substances (Lin and Yu, 2011; Verma et al., 2012), and quinones (Kumagai et al., 2002).

Quinones are a class of organic molecules derived from aromatic species, containing two carbonyl functionalities on a larger conjugated hydrocarbon ring. It has been suggested that redox cycling by quinone species within particles can lead to sustained oxidant generation once particles deposit within the body (Squadrito et al., 2001). A general redox cycle with a quinone species (1,2-naphthoquinone) is shown in Fig. 1; the ability of quinones to act as redox cycling agents lies in the stable semiquinone radical that is formed in the process. Quinones and their biochemistry have been well-studied and are known to be cytotoxic by both redox cycling reactions and their ability to conjugate with thiol groups (Gant et al., 1988).

Quinones are minor PM constituents, but due to their aforementioned potential to contribute to adverse health effects, their sources and ambient concentrations are important to understand. Quinones have been shown to be present in ambient particles (Cho et al., 2004; Chung et al., 2006; Valavanidis et al., 2006; Tsapakis and Stephanou, 2007; Eiguren-Fernandez et al., 2008a; Ahmed et al., 2009) and contribute to particle-bound stable radical species, as measured by electron paramagnetic resonance (Dellinger et al., 2001; Pan et al., 2004; Valavanidis et al., 2006). The source of these species may be primary or secondary. Specific quinones, including the redox-active 1,2-naphthoquinone, 1,4-naphthoquinone, and 9,10-phenanthrenequinone, have been measured as products in diesel and gasoline exhaust particles (Cho et al., 2004; Valavanidis et al., 2006; Jakober et al., 2007). They may also be produced as secondary products of polycyclic aromatic hydrocarbon (PAH) oxidation. Naphthalene (Bunce et al., 1997; Chan et al., 2009; Kautzman et al., 2010; Lee and Lane, 2009; Sasaki et al., 1997), phenanthrene (Lee and Lane, 2010; Wang et al., 2007), and anthracene (Kwamena et al., 2006) all generate their corresponding quinone species (naphthoquinone, phenanthrenequinone, and anthraquinone, respectively) via reaction with gas-phase oxidants. Formation of these species from PAH precursors in the atmosphere could increase the redox activity of ambient particles during photochemical aging in locations with PAH emission sources. Indeed, photochemical production of 9,10-phenanthrenequinone has been observed as air masses age in the Los Angeles basin (Eiguren-Fernandez et al., 2008b). It has also been observed that particles collected in the afternoon in Los Angeles tend to be higher in water soluble organic carbon, organic acids and redox activity, suggesting that secondary organic aerosol formation may contribute to redox activity of ambient particles (Verma et al., 2009).

Evidence of secondary organic aerosol contribution to redox activity has also been found from controlled oxidation studies. The redox activity of the water-soluble extract of particles formed from aging diesel exhaust particles with ozone in an outdoor chamber was about a factor of two higher than particles not exposed to ozone (Li et al., 2009). Additionally, modifying the VOC mix within the chamber could alter the amount by which water-soluble redox activity increased, regardless of the presence or absence of diesel exhaust particles in the chamber (Rattanavaraha et al., 2011). Previous experiments we have performed revealed that when two-stroke gasoline engine exhaust is oxidised with ozone, the redox activity that results can be modelled with a redox-active secondary organic aerosol that is over ten times more active per unit mass than the original primary engine particles (McWhinney et al., 2011).

While we know that PAH oxidation can generate quinone species and that quinones are efficient redox-cycling agents, very few studies so far have tried to extend this into examining our ability to predict and quantify the contribution of quinones to particle redox activity. In one such study researchers found that hydrogen peroxide generation from the DTT assay performed on particles from Fresno, California, could be accounted for by measuring the aerosol mass loadings of 9,10-phenanthrenequinone, 1,2-naphthoquinone, and 1,4-naphthoquinone (Chung et al., 2006). In another study, by assigning the DTT loss rate to individual particulate species again from the Fresno area, Charrier and Anastasio were able to predict DTT decay as arising 80 % from transition metal species and 20 % from quinone species (Charrier and Anastasio, 2012).

The aim of the current study was to examine to what extent redox behaviour can be predicted based on particulate mass loadings of 1,2-naphthoquinone, 1,4-naphthoquinone, and 9,10-phenanthrenequinone, i.e. the small, soluble quinones that are commonly associated with redox cycling. We have focussed on naphthalene secondary organic aerosol (SOA) generated by hydroxyl radical oxidation in a photoreaction chamber. Known to produce both 1,2 and 1,4 isomers of naphthoquinone (Lee and Lane, 2009), this provided a relatively simple system of redox-active aerosol generated through laboratory oxidation. The redox activity

of the particles was confirmed, and the extent to which these two naphthoquinone isomers contributed to observed redox cycling was examined based on quantification by gas chromatography-mass spectrometry. During the chamber experiments, we used online measurements taken with an aerosol mass spectrometer and a proton transfer reaction mass spectrometer to determine a gas–particle partitioning coefficient to explore the likely contribution of naphthoquinone species to ambient particle redox cycling behaviour. Through this work, we hope to gain a more thorough understanding of how well we understand organic redox cycling catalysis on a molecular basis and determine how well we know the inventory of redox-active organic products. As we further examine the photochemical processes that generate redox activity in particles, we can better predict the possible influences of aerosol aging on particle toxicity.

2 Experimental

2.1 Naphthalene SOA generation and collection

Chamber aerosol was generated by hydroxyl radical oxidation of naphthalene in a 1 m^3 Teflon (fluorinated ethylene propylene [FEP]) photoreaction chamber. The chamber is of a simple rectangular cuboid design with the inside of the chamber supported with a Teflon-wrapped metal frame and can be illuminated on four of the six faces with 24 ultraviolet lamps. Prior to particle generation, the chamber was flushed with several chamber volumes of zero air from an AADCO 737 Pure Air Generator. For the hydroxyl radical precursor, hydrogen peroxide was added to the chamber by bubbling zero air through a 30 % aqueous hydrogen peroxide solution (Sigma Aldrich) at a flow rate of approximately 400 cubic centimetres per minute (ccm) for one hour. Naphthalene was introduced to the chamber by vaporising a known mass of solid naphthalene (99 %, Acros Organics) in a flow of approximately 400 ccm of zero air.

Naphthalene concentrations in the chamber were monitored with an IONICON proton transfer reaction mass spectrometer (PTR-MS) equipped with a quadrupole mass spectrometer. Naphthalene and naphthoquinone concentrations were tracked by measuring the signal at mass-to-charge ratio (m/z) 129 and 159, respectively, as the singly protonated molecular ion. Once the PTR-MS naphthalene signal had stabilised in the chamber, indicating that mixing was complete, oxidation was initiated by illuminating the chamber with ultraviolet lamps with a peak emission at 310 nm (F40T12 UVB). Naphthalene concentrations were measured based on the PTR-MS signal calibrated to the known mass of naphthalene added to the chamber, assuming complete transfer and no wall loss. Hydroxyl radical concentrations are reported based on observed first order decay of naphthalene (transfer loss effects for naphthalene may affect the calibration, but this calibration does not affect any subsequent calculations discussed in this study). Stable naphthalene signals in the absence of oxidant indicated that hydroxyl radical oxidation is the only significant loss mechanism for naphthalene. Particles were formed by the nucleation of oxidised organics without addition of seed particles. The resultant SOA was characterised by an Aerodyne aerosol mass spectrometer (AMS) equipped with a high-resolution time-of-flight mass spectrometer and, in some instances, a scanning mobility particle sizer (SMPS) consisting of a differential mobility analyser (model 3081) and a condensation particle counter (TSI model 3025, Shoreview, MN, USA). Temperature was not controlled or monitored in the chamber but was typically slightly above room temperature due to heat from the UV lamps, at about 25 °C.

When the AMS exhibited maximum particle loading, which was typically 90–120 min after the beginning of the experiment, the lamps were turned off to stop the oxidation reaction. Particles were subsequently collected by pulling chamber air through Zefluor filters (Pall, polytetrafluoroethylene (PTFE), 47 mm diameter and 2 µm pore size) at a flow rate of 20 litres per minute (lpm). To prevent the chamber from collapsing, a 20 lpm zero air make-up flow was added to the chamber. In some experiments, gas-phase constituents were collected during this time by pulling an additional 1 lpm of chamber air through a PTFE filter to remove particles and then through an ORBO 43 Supelpak-20 cartridge (Sigma-Aldrich) containing two XAD-2 polystyrene resin beds in series. On average, more than 98 % of 1,4-naphthoquinone was collected on the front XAD bed, indicating that analyte breakthrough was not a concern. Together, these naphthalene SOA filter samples and gas-phase XAD cartridge samples were collected for 60–90 min and stored at −20 °C until further analysis.

2.2 DTT assay

The DTT analysis used was adapted from the procedure described by Cho et al. (2005), and was slightly modified from our previous work (McWhinney et al., 2011). Naphthalene SOA particle filter samples were divided into quarters and one quarter was extracted by mixing with 10 mL of phosphate buffer (0.1 M, pH 7.4). DTT (Sigma Aldrich) was added to 1 mL aliquots of the aqueous filter extracts to give a final volume of 1.25 mL and a DTT concentration of 0.1 mM. The redox reaction was performed at room temperature and quenched at 15 min intervals over the course of one hour by taking 0.25 mL aliquots of the DTT mixture and adding 1 mL of 0.25 mM 5,5'-dithiobis-(2-nitrobenzoic acid) (DTNB, Alfa Aesar). DTT was quantified by measuring the absorbance of the resulting product at 412 nm with a UV-Vis spectrophotometer. Redox activity is expressed as the time rate-of-change of DTT concentrations in M min^{-1} or as a particle mass normalised DTT decay rate in pmol min^{-1} μg^{-1}. DTT analysis was carried out on the filter extract without filtration of insoluble matter, as assay results

from extracts passed through a 0.2 µm PTFE syringe filter showed that 96 % of the naphthalene SOA redox activity was found in the water-soluble fraction of the extract (McWhinney et al., 2013).

2.3 Quinone analysis

Quinones were quantified by gas chromatography-mass spectrometry (GC-MS) using the derivatisation method from Cho et al. (2004). A one-quarter portion of the filter was extracted directly with dichloromethane (approximately 0.5 mL) by sonication for 15 min in a glass centrifuge tube. Menadione (2-methyl-1,4-naphthoquinone, Sigma Aldrich) was added to each extract as an internal standard. The quinone species were derivatised using reductive acetylation, wherein the quinone is reduced to the hydroquinone functionality in the presence of zinc and esterified in the presence of acetic anhydride (see Fig. 2). The derivatisation was performed by adding 0.5 mL of acetic anhydride (ACP Chemicals) and approximately 100 mg of powdered zinc (Sigma Aldrich) to the dichloromethane extract. The mixture was heated to 80 °C and mixed every five minutes. After 15 min, the reaction was cooled, an additional 100 mg of zinc was added, and the mixture was heated for another 15 min. After cooling, the remaining acetic anhydride was quenched with 1 mL of deionised water and the diacetylated quinones were extracted with 3 mL of pentane. After shaking, the mixture was centrifuged and the top organic layer was removed, dried under a stream of nitrogen, and reconstituted in 100 µL of dichloromethane. The dichloromethane mixture was analysed by GC-MS using the parameters in Table 1. Calibration standards of 1,2-naphthoquinone, 1,4-naphthoquinone, and 5-hydroxy-1,4-naphthoquinone (Sigma Aldrich) were prepared using the same procedure. The calibration was performed in each case based on the fully deacetylated fragment ion. Limits of quantification were operationally defined as the lowest standard concentration used for calibration, corresponding to quinone masses of 0.2 µg per full filter for naphthalene SOA samples.

2.4 Gas–particle partitioning coefficient calculation

The gas–particle partitioning coefficient of 1,4-naphthoquinone was determined using the equation $K_p = c_p/(M_p c_g)$ (Pankow, 1994) where c_p and c_g are the concentrations of 1,4-naphthoquinone in the particle phase and the gas phase, respectively, and M_p is the mass loading of the particles in the chamber. The concentration of 1,4-naphthoquinone in the gas phase was calculated from the PTR-MS signal at m/z 159 ($[M+H]^+$), and the concentration in the particle phase was determined from the AMS signal at m/z 158 (M^+). The PTR-MS response was calibrated by comparison with the quantified 1,4-naphthoquinone from the XAD cartridge samples assuming full recovery of 1,4-naphthoquinone, while AMS signals

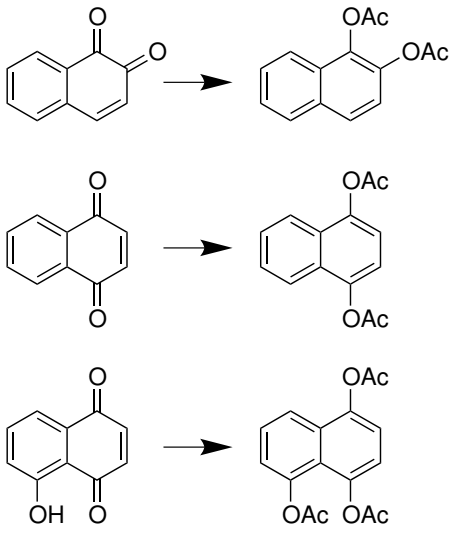

Fig. 2. 1,2-naphthoquinone (top left), 1,4-naphthoquinone (middle left), and 5-hydroxy-1,4-naphthoquinone (bottom left) and their respective acetylated derivatives (right).

were calibrated with the quantified 1,4-naphthoquinone from filter samples ($r^2 = 0.9$ for PTR-MS calibration and $r^2 = 0.6$ for AMS calibration). The particulate mass loading was taken as the total organics measured by the AMS. To correct for particle bounce due to the low relative humidities used in the experiments, a collection efficiency of 0.5 was used for all AMS data. To verify the suitability of this choice, AMS mass loadings were compared to mass loadings calculated from SMPS-measured particle volumes using a particle density of 1.55 g cm^{-3} (Chan et al., 2009); good agreement between the two values was obtained using 0.5 as the AMS collection efficiency.

3 Results and discussion

3.1 Redox activity prediction for naphthalene SOA

We are interested in determining how well we can predict the redox activity of secondary organic aerosol particles using molecular-level information on the activities and loadings of known quinones. To start with as simple a system as possible by using only one SOA precursor, naphthalene was chosen for its ability to form aerosol in relatively high yield – particularly under low NO_x conditions (Chan et al., 2009) – which was advantageous for the small size of our photoreaction chamber. The mass spectrum of the SOA generated in the chamber was fairly invariable from day-to-day and consisted mostly of hydrocarbon (C_xH_y) and oxidised hydrocarbon ($C_xH_yO_z$) fragments; elemental composition information is given in Table 2, as obtained using established methods (DeCarlo et al., 2006; Aiken et al., 2007), and the average AMS mass spectrum from two representative experiments is shown

Table 1. GC-MS method parameters as adapted from Cho et al. (2004).

Gas chromatograph	Agilent 7890A Agilent 7683 Series autosampler
Inlet temperature and pressure	260 °C, 10.5 psi
Injection	1 µL, pulsed splitless injection at 25 psi for 0.5 min
Carrier gas	He, 10.5 psi, 1 mL min^{-1} flow rate
Run time	40 min
Temperature program	100 °C, hold 4 min 5 °C min^{-1} to 280 °C
Mass spectrometer	Agilent 5975C
Ionisation mode	Electron impact

Time	Selected ions (m/z)
22–25.5 min	160 ($[M-2CH_2CO]^+$), 202 ($[M-CH_2CO]^+$), 244 ($[M]^+$)
25.5–30 min	174 ($[M-2CH_2CO]^+$), 216 ($[M-CH_2CO]^+$), 258 ($[M]^+$)
30–34 min	176 ($[M-3CH_2CO]^+$), 218 ($[M-2CH_2CO]^+$), 260 ($[M-CH_2CO]^+$), 302 ($[M]^+$)

Table 2. Average elemental composition of particles at the end of the photooxidation portion of the experiment.

H : C ratio	0.97 ± 0.08
O : C ratio	0.31 ± 0.02
N : C ratio	0.03 ± 0.01
C_xH_y mass contribution	(31 ± 1) %
$C_xH_yO_1$ mass contribution	(23 ± 1) %
$C_xH_yO_{>1}$ mass contribution	(18 ± 1) %
C_xH_yN mass contribution	(3 ± 2) %
$C_xH_yO_1N$ mass contribution	(1.2 ± 0.3) %
$C_xH_yO_{>1}N$ mass contribution	(0.36 ± 0.09) %
HO mass contribution	(5 ± 2) %

in Fig. 3. There was an unexpected small fraction of the particle mass made up of C_xH_yN type fragments potentially as a result of amine contamination in the chamber, which was previously used for the photooxidation of ethanolamine. These peaks make up approximately only 3 % of the organic mass, on average, for an overall N : C ratio of approximately 0.03. It is currently unknown what types of species would be contributing these fragments to the overall mass spectrum.

SOA generated from naphthalene oxidation was expected to exhibit high redox activity, based on knowledge that both 1,2- and 1,4-naphthoquinone isomers could be found in the particle phase as naphthalene oxidation products (Lee and Lane, 2009). The particles generated from naphthalene oxidation were highly redox active and reflective of the reproducible composition; DTT decay rates were reasonably invariant with an average DTT decay per unit mass of particle of 118 ± 14 pmol min^{-1} μg^{-1} ($n = 10$; individual experimental results are summarised in Table 3). As a comparison, we previously estimated the activity of the two-stroke engine exhaust SOA to be 8.6 ± 2.0 pmol min^{-1} μg^{-1} (McWhinney et al., 2011).

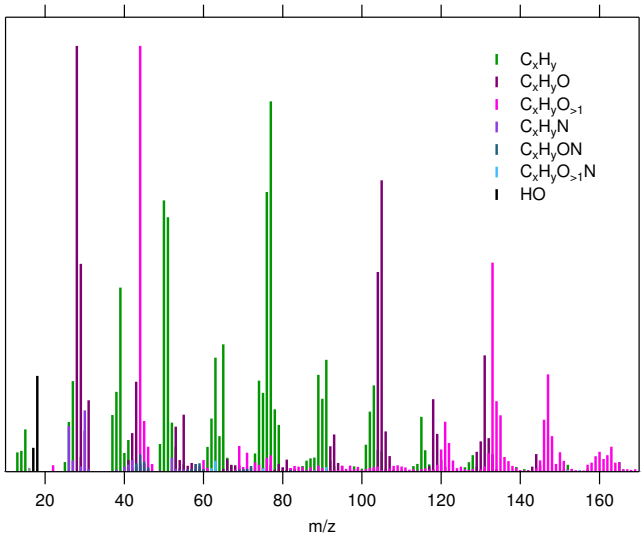

Fig. 3. Average mass spectrum of naphthalene SOA coloured by fragment family.

For prediction of the SOA activity, we focussed on the 1,2- and 1,4-naphthoquinone isomers, which as mentioned in the Introduction, along with 9,10-phenanthrenequinone, are commonly believed to be the most important water soluble quinone electron transfer agents (e.g. Chung et al., 2006; Charrier and Anastasio, 2012). As mentioned in the Experimental section, the quinones were extracted directly from the filter using dichloromethane rather than measuring the water-soluble species, so it is assumed that the efficiency of quinone extraction was equal for phosphate buffer and dichloromethane.

Both 1,2- and 1,4-naphthoquinone were detected in the particle phase at mass loadings of a similar magnitude (see Table 3). Each run of the DTT assay included positive controls containing only 1,2- or 1,4-naphthoquinone in

Table 3. Summary of DTT and quinone analysis for naphthalene oxidation experiments.

	DTT decay rates				Particulate quinone masses[c,d]			
Experiment	Measured[a]/ 10^{-7} M min^{-1}	Mass normalised/ pmol min^{-1} µg^{-1}	Predicted[b]/ 10^{-7} M min^{-1}	Predicted[b] with 5-OH-1,4-NQ/10^{-7} M min^{-1}	1,4-NQ /µg	1,2-NQ /µg	5-OH-1,4-NQ /µg	PM mass[d] /mg
May 27	6.1 ± 0.8	116 ± 16	1.4 ± 0.2	–[e]	4.3 ± 0.4	1.2 ± 0.1	–	0.44
May 31	8.1 ± 0.9	104 ± 12	2.2 ± 0.3	–	6.6 ± 0.6	2.2 ± 0.3	–	0.65
Jun 1	5.7 ± 0.9	122 ± 20	1.1 ± 0.2	–	3.7 ± 0.3	0.9 ± 0.1	–	0.39
Jun 2A	7.0 ± 1.0	130 ± 19	1.5 ± 0.3	–	3.7 ± 0.3	2.3 ± 0.3	–	0.45
Jun 2B	7.1 ± 1.0	87 ± 8	1.5 ± 0.3	–	3.2 ± 0.3	2.6 ± 0.3	–	0.68
Jun 3	7.0 ± 0.9	140 ± 18	1.5 ± 0.3	–	4.8 ± 0.4	1.3 ± 0.2	–	0.42
Aug 3A	5.2 ± 1.1	121 ± 25	1.3 ± 0.3	1.7 ± 0.4	2.3 ± 0.2	2.0 ± 0.2	0.7 ± 0.2	0.54
Aug 3B	3.3 ± 1.3	113 ± 43	0.7 ± 0.2	1.2 ± 0.3	1.5 ± 0.1	1.1 ± 0.1	0.8 ± 0.2	0.37
Aug 4A	3.1 ± 1.2	125 ± 47	0.5 ± 0.1	0.9 ± 0.2	1.2 ± 0.1	0.8 ± 0.1	0.6 ± 0.2	0.31
Aug 4B	5.9 ± 1.2	125 ± 25	1.0 ± 0.3	1.4 ± 0.3	1.8 ± 0.2	1.7 ± 0.2	0.5 ± 0.2	0.59

[a] Measured reported is based on dilution of the extract used in the assay for a particular sample and will not scale directly with reported quinone or PM masses.
[b] Predicted values match dilution factors used in the measured assay.
[c] Quinone masses for 1,4-naphthoquinone (1,4-NQ), 1,2-naphthoquinone (1,2-NQ) and 5-hydroxy-1,4-naphthoquinone (5-OH-1,4-NQ) are corrected using spike and recovery measurements.
[d] Mass reported is for whole filter.
[e] 5-hydroxy-1,4-naphthoquinone not measured.

phosphate buffer to determine the mass-dependent DTT decay rates for these species for any given set of assay runs. The activities of the positive controls were used to calculate the expected DTT decay of each SOA filter extract based on the measured naphthoquinones in the dichloromethane extract. The predicted values based on 1,2- and 1,4-naphthoquinone particulate concentrations are plotted against the measured redox activity in Fig. 4 assuming the redox activities are additive, as was reported for quinone species in the supporting information of Charrier and Anastasio (2012). There is a strong correlation between the predicted and observed DTT decay rates ($r^2 = 0.87$). However, predicted DTT decay rates fall considerably below those observed. After correction for recovery (measured for 1,2- and 1,4-naphthoquinone as 83 ± 10 % and 87 ± 8 %, respectively), predicted values accounted for 21 ± 3 % of the measured values.

Based on the measured loadings of the two naphthoquinone isomers on the filters, we are considerably underestimating the observed redox activity of the aqueous filter extracts. One possible explanation for this discrepancy could be poor extraction of the quinone species using the dichloromethane extraction method compared to the aqueous extraction method. Considering the high solubility of naphthoquinone in dichloromethane and the aforementioned reasonable recoveries from spiked filters, this is not believed to be the cause of the discrepancy. Rather, we postulate that there are other species in the naphthalene SOA exhibiting redox activity.

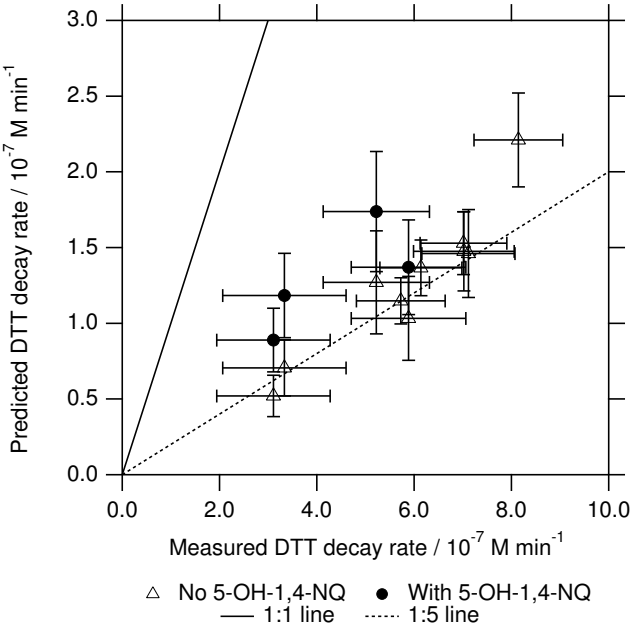

Fig. 4. Predicted DTT decay rates of naphthalene SOA filter extracts plotted against the measured DTT decay rates. Open triangles represent predicted values based on measured 1,2- and 1,4-naphthoquinone on the particle filters, while filled circles also include 5-hydroxy-1,4-naphthoquinone (5-OH-1,4-NQ) in the prediction. A 1 : 1 line indicates the expected relationship if predicted DTT decay rates equal those observed.

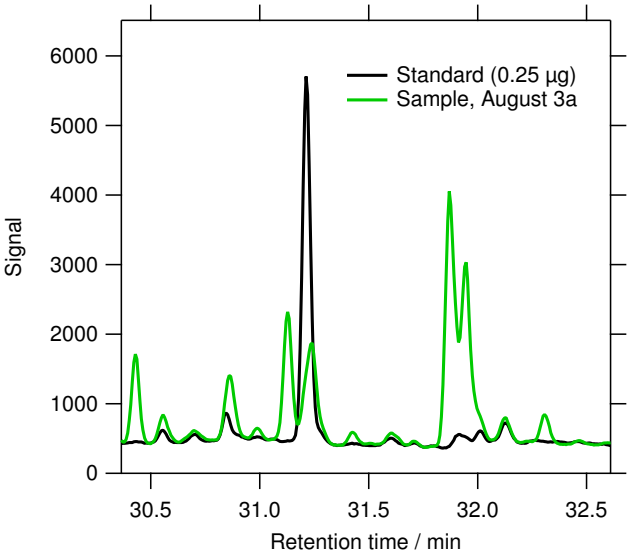

Fig. 5. Sample chromatogram for 5-hydroxy-1,4-naphthoquinone ($t_R = 31.2$ min) for the m/z 176 fragment (loss of three acetyl groups from molecular ion).

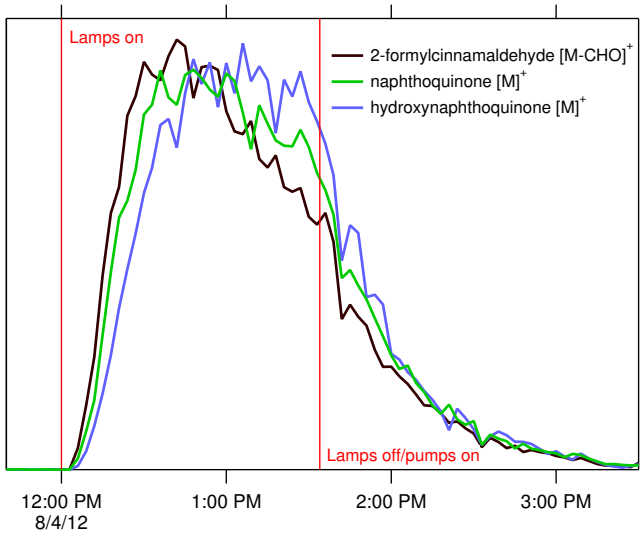

Fig. 6. Time series of high-resolution AMS data for $C_9H_7O^+$ (2-formylcinnamaldeyde $[M-CHO]^+$), $C_{10}H_6O_2^+$ (naphthoquinone $[M]^+$), and $C_{10}H_6O_3^+$ (hydroxynaphthoquinone $[M]^+$). Signals have been scaled to appear the same magnitude.

3.2 Redox activity of naphthoquinone analogues

The rate of quinone redox cycling is determined primarily by the one-electron redox potential of the various species. For example, it has been previously shown that the logarithm of the rate constant of the reaction between a reducing agent, ascorbate, and a given quinone species is linearly related to the one-electron reduction potential of the conversion of the quinone to its corresponding semiquinone radical anion (Roginsky et al., 1999). Therefore, quinones with low one-electron reduction potentials are likely to exhibit slower redox cycling rates than those with higher potentials. With 1,4- and 1,2-naphthoquinones having one-electron reduction potentials of −140 mV and −89 mV, respectively (Wardman, 1989), we have looked for plausible products of the reaction of naphthalene and hydroxyl radical with a similar reduction potential that have not been previously identified in product studies. Specifically, the presence of 5-hydroxy-1,4-naphthoquinone and 5,8-dihydroxy-1,4-naphthoquinone – with reduction potentials of −93 mV and −110 mV, respectively (Wardman, 1989) – were examined due to the plausibility of these compounds as third and fourth generation oxidation products of naphthalene.

The 5-hydroxy-1,4-naphthoquinone product (but not 5,8-dihydroxy-1,4-naphthoquinone) was identified and quantified in the naphthalene SOA particles by GC-MS, confirmed by retention time (Fig. 5) and fragmentation pattern. To the best of our knowledge, this is the first time this product had been identified in secondary organic aerosol produced from the oxidation of naphthalene. Like 1,4-naphthoquinone, 5-hydroxyl-1,4-naphthoquinone has a considerable signal at the molecular ion in the electron impact mass spectrum (NIST Mass Spec Data Centre, 2013). We compared the AMS time series data for the first generation product 2-formylcinnamaldehyde through the m/z 131 $[M-CHO]^+$ ($C_9H_7O^+$) fragment (NIST Mass Spec Data Centre, 2013), the second generation product 1,4-naphthoquinone molecular ion at m/z 158 ($C_{10}H_6O_2^+$), and the expected m/z 174 signal for the molecular ion of 5-hydroxy-1,4-naphthoquinone ($C_{10}H_6O_3^+$) from high-resolution data (i.e. excluding other ions at each nominal mass). The temporal trends, shown in Fig. 6, are supportive of the production of first generation 2-formylcinnamaldehyde, second generation 1,4-naphthoquinone, and third generation 5-hydroxy-1,4-naphthoquinone in the particle phase, with each rising and falling in concentration progressively later in the experiment.

As is anticipated from a probable third generation oxidation product of naphthalene, the yield of 5-hydroxy-1,4-naphthoquinone is somewhat lower compared to the second generation 1,2- and 1,4-naphthoquinones. The molecule was not detected in gas-phase XAD samples from the chamber and particle-phase loadings were on average about 41 % of 1,4-naphthoquinone and 55 % of 1,2-naphthoquinone after correction using an average recovery of 40 ± 12 % from spike and recovery measurements. While 5-hydroxy-1,4-naphthoquinone is a minor contributor in terms of aerosol mass, the redox activity of 5-hydroxy-1,4-naphthoquinone is higher than that of the other two quinone species (about 7.8 pmol min^{-1} ng^{-1} compared to 2.1 and 5.7 pmol min^{-1} ng^{-1} for 1,4- and 1,2-naphthoquinone, respectively). The 5-hydroxy-1,4-naphthoquinone accounts for, on average, 33 % of the predicted redox activity in the

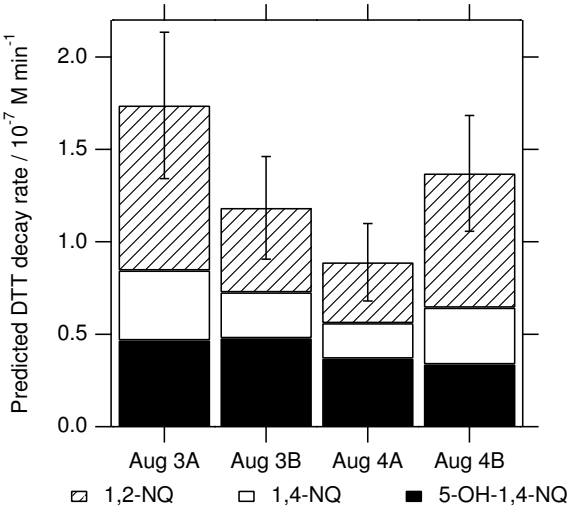

Fig. 7. Predicted DTT decay rates by constituent for four experiments (labelled A–D) where 1,2-, 1,4-, and 5-hydroxy-1,4-naphthoquinone (1,2-NQ, 1,4-NQ, and 5-OH-1,4-NQ, respectively) were quantified in the particle phase.

particles (Fig. 7). Including 5-hydroxy-1,4-naphthoquinone in the predicted DTT decay rates, closure improves to 30 ± 5 % in Fig. 4 (versus 20 ± 3 % for 3 and 4 August filter samples using only 1,2- and 1,4-naphthoquinone to predict redox activity).

The recovery of 5-hydroxy-1,4-naphthoquinone was low and variable compared to 1,2- and 1,4-naphthoquinone; it is possible that this may have resulted in an overestimation in particulate mass loadings for this species (and subsequently the relative contribution of the molecule to the measured redox cycling rates). As such, the numbers reported for this species above may be considered as an upper limit. Regardless, this product is significant in terms of overall redox cycling. If the redox activity of the particles is calculated without correcting for different recoveries, 5-hydroxy-1,4-naphthoquinone is still expected to account for about 19 % of the predicted redox cycling on average. It is not implausible that other functionalised naphthoquinone species contribute small amounts to the unaccounted redox cycling activity. It is beyond the scope of the current project to identify remaining redox-active species, but we note that there are very likely as-of-yet unidentified redox-active organic compounds that could contribute to redox cycling in particulate matter in addition to the three small quinone species that have been the subject of previous focus.

3.3 Air-particle partitioning of 1,4-naphthoquinone

The degree to which the redox-active naphthoquinone products influence the toxicity of particles depends on the partitioning behaviour of the compounds. The drawback of chamber photooxidation studies is that particle mass loadings are typically many times higher than those observed under ambient conditions, which tends to favour partitioning to the particle phase. In the current experiments, particle mass loadings were on the order of several hundreds of micrograms per cubic metre, and so whether or not 1,2- or 1,4-naphthoquinone partition to the particle phase in significant enough quantities to be of concern to health under typical ambient conditions is an important question. Gas–particle partitioning coefficients allow some estimation of how important naphthoquinone photooxidation is to the health impact of particulate matter, particularly in urban areas where anthropogenic emissions of naphthalene are important. Only one study has previously reported a gas–particle partitioning coefficient for 1,4-naphthoquinone, which was in diesel exhaust particles (Jakober et al., 2007). We aim to verify the partitioning behaviour of 1,4-naphthoquinone in a system with only organic carbon aerosol and without potential interference from adsorption into the black carbon found in diesel particles.

The gas- and particle-phase concentrations of 1,4-naphthoquinone were obtained from the PTR-MS and AMS measurements, respectively. In order to do so, a number of assumptions needed to be made. First, all AMS signal at m/z 158 was assumed to come from the $C_{10}H_6O_2^+$ ion, which is the molecular ion of naphthoquinone. As the ionisation efficiency calibration was more reliable for the lower-resolution V-mode data from the AMS (using a shorter V-shaped ion time-of-flight region), these data were used to calculate the total masses of naphthoquinone and total SOA mass loading. Higher resolution W-mode data from the AMS (using a longer W-shaped ion time-of-flight region) confirmed that, on average, 90 % of the signal at m/z 158 came from the $C_{10}H_6O_2^+$ ion, allowing the unit-mass resolution data from m/z to be used with an error of approximately 10 %.

The second assumption was that the AMS was sensitive to the 1,4 isomer but not the 1,2 isomer of naphthoquinone. This is based on the thermal instability of 1,2-naphthoquinone. Thermal analysis of quinones revealed that while 1,4-naphthoquinone exhibits thermal stability up to 600 °C, 1,2-naphthoquinone begins decomposing at temperatures higher than 100 °C, and the thermal instability was verified by very poor reproducibility in GC-MS analysis (Sousa et al., 2012). The authors attributed the thermal instability to the carbonyl groups of the quinones being in the ortho position to each other, as 9,10-phenanthrenequinone also exhibited thermal instability. We postulate that 1,2-naphthoquinone was only recently identified in naphthalene SOA (Lee and Lane, 2009) due to the tendency of the 1,2 isomer to degrade under the GC-MS conditions normally used to separate and measure quinone species, particularly at high injector temperatures. As such, we are only able to detect 1,2-naphthoquinone by GC-MS when using the reductive acetylation derivatisation technique.

With the approximately 600 °C temperature of the AMS vapouriser, 1,2-naphthoquinone is not expected to be observable by the AMS. To verify this, each of the naphthoquinone

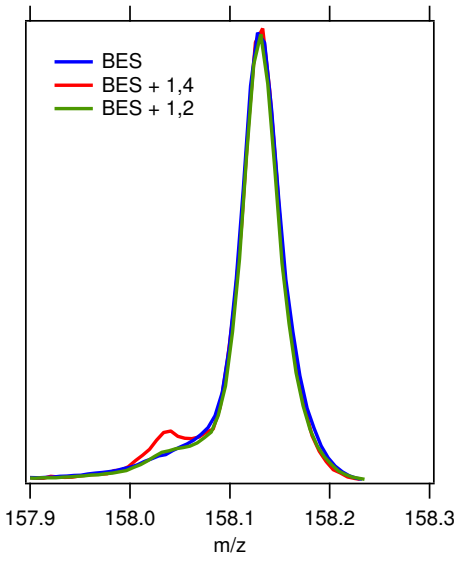

Fig. 8. Raw mass spectra at m/z 158 for homogeneously nucleated BES without naphthoquinone and with 1,4-naphthoquinone and 1,2-naphthoquinone. The peak of the highest intensity arises from a $C_9H_{18}O_2^+$ fragment from BES (actual mass 158.131 amu), while the small peak seen in the red trace arises from the $C_{10}H_8O_2^+$ molecular ion of 1,4-naphthoquinone (actual mass 158.037 amu).

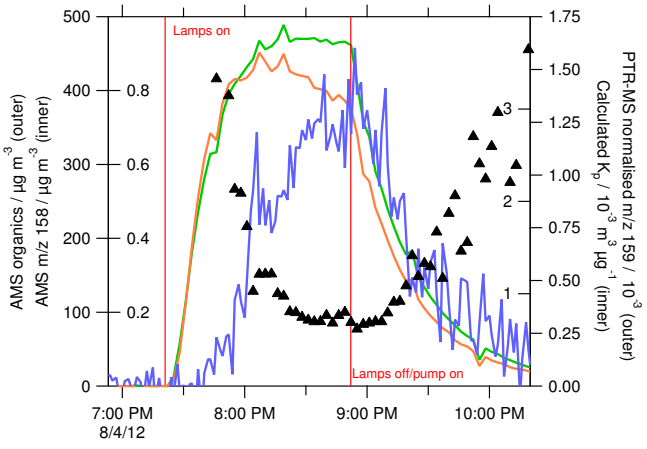

Fig. 9. Representative experimental data for a naphthalene generation experiment. AMS organics (green) and m/z 158 (orange) were corrected for a collection efficiency of 0.5. The PTR-MS signal for protonated naphthoquinone at m/z 159 (blue) was normalized to the reagent ion count. The gas–particle portioning coefficient K_p (black triangles) was calculated for each time point using AMS and PTR-MS data calibrated to filter and XAD measurements of 1,4-naphthoquinone, respectively.

isomers were separately mixed with a high molecular weight oil, bis(2-ethylhexyl) sebacate (BES). The mixtures were heated to homogeneously nucleate particles, which were subsequently sampled under the high-resolution mode of the AMS. Signals at m/z 158 from BES without quinone and with the 1,4 and 1,2 isomers are shown in Fig. 8. As hypothesised, the BES with 1,4-naphthoquinone exhibited signal at a nominal mass of 158 corresponding to the $C_{10}H_6O_2^+$ molecular ion, which is partially obscured by signal from BES (from a fragment of $C_9H_{18}O_2^+$). A signal for this ion was not observed for 1,2-naphthoquinone. Based on these results, we believe 1,2-naphthoquinone is likely to thermally decompose upon making contact with the AMS vapouriser and that the signal from the naphthoquinone molecular ion can be attributed to the 1,4 isomer. Reasonable correlation between the AMS m/z 158 signal with 1,4-naphthoquinone filter measurements ($r^2 = 0.6$) was obtained.

The third assumption made was that the PTR-MS signal primarily arises from gas-phase 1,4-naphthoquinone. The reliability of this assumption depends on the relative amounts of 1,2-naphthoquinone and 1,4-naphthoquinone in the gas phase. Previous studies have found that in the gas phase, concentrations of the 1,2 isomer are lower than for the 1,4 isomer in both chamber (Lee and Lane, 2009) and ambient (Eiguren-Fernandez et al., 2008a) particles. This observation held true with our chamber experiments, with the ratio of the 1,2 to 1,4 naphthoquinone isomers being 0.015 ± 0.010 in the gas phase. Based on this observation, attributing the PTR-MS signal to 1,4-naphthoquinone is a reasonable assumption. Calibration using five experiments with collected XAD cartridges yielded a strong correlation between the PTR-MS data and the 1,4-naphthoquinone extracted from the XAD resin ($r^2 = 0.90$).

Finally, some evidence of equilibrium must be exhibited to properly calculate a partitioning coefficient assuming partitioning into a bulk phase. The low relative humidity in the chamber is likely to result in particles that are not liquid, but equilibrium can be established over appreciable periods of time if the particles are at least semi-solid with fast enough diffusion in the bulk. Indeed, during the course of an experiment, the calculated values for the gas–particle partition coefficient were not constant, but tended towards a stable value near the time when the lights are turned off in the chamber, as illustrated in Fig. 9. The stable value indicated that the system likely reached equilibrium by the end of a typical 90 min experiment. Using a time scale of diffusion of $\tau = d^2/(4\pi D)$, a time scale of 90 min corresponds to a diffusion coefficient of approximately 2×10^{-15} cm^2 of 1,4-naphthoquinone in the SOA particle, which is within the range expected for a semi-solid particle (Shiraiwa et al., 2011). As such, the conditions to assume equilibrium partitioning in the bulk phase appear to be met.

We obtained an average partitioning coefficient for a single experiment by averaging the values taken over a 10 min period prior to the lamps being turned off: $(7.0 \pm 2.5) \times 10^{-4}$ m^3 µg^{-1}; the uncertainty is based on the standard deviation of all experiments, for which the results are summarised in Table 4. As the PTR-MS was calibrated assuming full recovery of 1,4-naphthoquinone from the XAD cartridge,

Table 4. Summary of AMS and PTR-MS measurements for naphthalene oxidation experiments.

Experiment	$[OH]^a/10^7$ molec cm^{-3}	$[Naphthalene]_i^b$ /ppb	$[1,4\text{-NQ}]_{g,f}^{c,d}$ /μg m^{-3}	$[1,4\text{-NQ}]_{p,f}^{c,e}$ μg m^{-3}	$M_p^{c,f}$ μg m^{-3}	K_p^d /10^{-4} m^3 μg^{-1}
Apr 17	1.1	480 ± 50	29.7 ± 2.3	3.8 ± 0.9	443 ± 89	2.7 ± 0.3
May 14	1.2	279 ± 29	23.5 ± 1.8	2.5 ± 0.6	281 ± 56	3.7 ± 0.2
May 27	1.1	251 ± 26	18.7 ± 3.2	2.8 ± 0.7	323 ± 65	5.0 ± 1.1
May 28A	1.6	225 ± 23	14.7 ± 2.2	3.3 ± 0.8	417 ± 83	4.9 ± 0.5
May 28B	1.6	237 ± 25	16.5 ± 2.3	3.0 ± 0.7	383 ± 77	4.8 ± 0.4
May 29A	1.7	282 ± 29	18.9 ± 1.3	4.0 ± 1.0	516 ± 103	4.0 ± 0.4
May 29B	1.9	181 ± 19	9.2 ± 0.8	2.7 ± 0.7	367 ± 73	7.6 ± 0.4
May 31	1.6	267 ± 28	12.3 ± 1.4	4.0 ± 1.0	514 ± 103	6.2 ± 0.5
Jun 1	1.9	136 ± 14	6.6 ± 1.2	2.3 ± 0.6	315 ± 63	9.3 ± 2.5
Jun 24A	1.0	257 ± 27	7.8 ± 1.7	3.2 ± 0.8	344 ± 69	10.4 ± 1.7
Jun 24B	1.4	233 ± 24	11.6 ± 0.9	3.5 ± 0.9	417 ± 83	6.9 ± 1.7
Jul 24	1.2	251 ± 26	10.6 ± 1.7	3.2 ± 0.8	333 ± 67	8.4 ± 0.7
Jul 25A	1.9	157 ± 16	6.5 ± 0.9	2.1 ± 0.5	281 ± 56	10.1 ± 1.8
Jul 25B	1.0	361 ± 37	14.5 ± 2.1	4.2 ± 1.0	455 ± 91	5.6 ± 0.7
Aug 3A	1.0	302 ± 31	7.1 ± 2.1	4.3 ± 1.1	463 ± 93	10.7 ± 1.7
Aug 3B	1.6	244 ± 25	8.5 ± 1.1	2.5 ± 0.6	318 ± 64	8.4 ± 0.7
Aug 4A	1.5	169 ± 18	7.2 ± 0.8	1.8 ± 0.4	231 ± 46	9.7 ± 1.5
Aug 4B	1.3	315 ± 33	10.4 ± 0.8	3.8 ± 0.9	467 ± 93	7.5 ± 0.5

[a] Calculated from first-order decay of naphthalene ($k_{OH} = 2.2 \times 10^{-11}$ molec^{-1} cm^{-3}, Sasaki et al., 1997); relative standard deviation of fit was typically less than ±1 %.
[b] Uncertainty based on ±10 % relative standard deviation of PTR-MS calibration for naphthalene.
[c] Values averaged from 10 min of data prior to lamp shutoff time.
[d] Uncertainty based on standard deviation of averaged values 10 min prior to lamp shutoff.
[e] Uncertainty based on a ±25 % relative standard deviation of the calibration slope for calculation of 1,4-naphthoquinone from AMS m/z 158.
[f] Uncertainty estimated at ±20 %.

this may be a lower limit. This is a larger value than those estimated by the EPI Suite software, likely due to the potential for inaccurate predictions from structural activity relationships; the McKay model predicts a value of 1.24×10^{-5} m^3 μg^{-1}, while the octanol-air model predicts a value of 1.56×10^{-4} m^3 μg^{-1} (US EPA, 2013). However, this value is in good agreement with the previously mentioned value of 4×10^{-4} m^3 μg^{-1} reported for 1,4-naphthoquinone organic matter partitioning in diesel exhaust particles (Jakober et al., 2007).

3.4 Air-particle partitioning of 1,2-naphthoquinone

A corollary to the assumptions we made to calculate the 1,4-naphthoquinone partitioning coefficient is that we cannot use a similar technique to calculate a partitioning coefficient for 1,2-naphthoquinone. This is unfortunate, as we have found, like earlier studies (Lee and Lane, 2009; Eiguren-Fernandez et al., 2008a), that the 1,2 isomer of naphthoquinone partitions to the particle phase to a greater extent than the 1,4 isomer. As discussed by Lee and Lane (2009), the ratio of 1,2- to 1,4-naphthoquinone tends to be higher in the particle phase than in the gas phase. The ratio of the 1,2 to 1,4 isomers we have measured in the gas phase and in the particle phase is 0.015 ± 0.010 (as mentioned previously) and 0.58 ± 0.27, respectively, indicating that 1,2-naphthoquinone is much more abundant in the particulate phase. This is despite previous reports that the vapour pressure of the 1,2 isomer is higher than that of the 1,4 isomer (Jakober et al., 2007; Lee and Lane, 2009), although based on the Modified Grain method structural activity relationship from the EPI Suite software package, where the calculated vapour pressures at 25 °C are 1.08×10^{-4} torr and 1.69×10^{-4} torr for 1,2 and 1,4 naphthoquinone, respectively (US EPA, 2013), partitioning trends are consistent with vapour pressure. The ratios themselves are lower than the range of values summarised in Lee and Lane (2009), which suggests that the yield of 1,2-naphthoquinone relative to 1,4-naphthoquinone in our system is lower than in other studies. As those values are taken from engine samples, urban PM, and high-NO_x chamber studies, this may be attributed to the low-NO_x conditions used in this study. Regardless, our findings agree that the vapour pressure of 1,2-naphthoquinone is in fact lower than that of 1,4-naphthoquinone based on the partitioning behaviour between the gas and particle phases, and thus 1,2-naphthoquinone is potentially of more interest in the particle phase than 1,4-naphthoquinone.

It is somewhat unsatisfactory to use the filter and XAD cartridge data to estimate the partitioning coefficient for 1,2-naphthoquinone, as during the filter collection period, the system deviates from equilibrium. The calculated partitioning coefficient increases as the chamber is pumped,

presumably due to dilution rates of the particles occurring on a faster time scale than the diffusion of 1,4-naphthoquinone out of the particle that is required to re-establish equilibrium. In absence of appropriate measurements, the ratio of the 1,2 to 1,4 isomers can be used to obtain an estimate of the partitioning coefficient by combining partitioning coefficient expressions for the two species to give $K_{p1,2} = K_{p1,4}(r_p/r_g)$, where r_p and r_g are the ratio of the 1,2 to the 1,4 isomer of naphthoquinone in the particulate and gaseous phases, respectively. Using data from our chamber, the value for K_p is estimated to be $(3.8 \pm 2.7) \times 10^{-2}\,m^3\,\mu g^{-1}$; this calculation was performed using only experimental data that included simultaneous gas- and particle-phase measurements. Using ratios obtained in other studies, we obtained values of $(5.3 \pm 4.6) \times 10^{-3}\,m^3\,\mu g^{-1}$ (Lee and Lane, 2009) and $(3.6 \pm 2.2) \times 10^{-3}\,m^3\,\mu g^{-1}$ (Eiguren-Fernandez et al., 2008a).

We note that the estimate based on our data is approximately an order of magnitude higher than when we use the values from other studies. As the Lee and Lane (2009) values are obtained from a larger chamber that does not require dilution during particle sampling, and as the Eiguren-Fernandez et al. (2008a) values are taken from ambient particles, these values are more likely to be taken under equilibrium conditions. Given the close agreement between these estimated coefficients, we consider the calculations using the Lee and Lane (2009) and the Eiguren-Fernandez et al. (2008a) values to be a more reliable estimate of the gas–particle partitioning coefficient for 1,2-naphthoquinone.

4 Atmospheric implications

Naphthoquinones are already known to be minor contributors to particle mass, and as such the generation of quinone species is not a concern to SOA mass loadings. However, due to high SOA mass yields, naphthalene itself has a potential to contribute considerably to particulate mass in areas with strong PAH emissions. For example, it has been estimated that naphthalene, 1- and 2-methylnaphthalene, acenaphthalene and acenaphthylene from mobile sources could contribute 37–162 $kg\,m^{-3}\,d^{-1}$ of SOA in Houston, Texas, compared to a total SOA estimate of 268 $kg\,m^{-3}\,d^{-1}$ from mobile sources, with a substantial fraction (36–48 %) of the PAH SOA mass coming from naphthalene oxidation (Shakya and Griffin, 2010). For diesel exhaust, it was estimated that of SOA production from oxidation of light aromatics, PAHs, and long-chain alkanes, 58 % of the aerosol produced arises from PAH precursor species (Chan et al., 2009). With a significant amount of naphthoquinone production from naphthalene oxidation and sufficient organic aerosol mass loading available for gas–particle partitioning, naphthoquinones may have a significant impact in terms of the redox behaviour and toxicity of ambient particles.

There are few studies that have attempted to model the atmospheric burden of 1,4-naphthoquinone. One study modelled the atmospheric burden resulting from oxidation of naphthalene and 1-naphthol and the photolysis of 1-nitronaphthalene in Southern California, and much of central Los Angeles was predicted to have 1,4-naphthoquinone concentrations in excess of 0.5 $ng\,m^{-3}$ and up to 2.5 $ng\,m^{-3}$ based on modelled naphthalene emissions for a week in July 1998 (Lu et al., 2005). These values are similar in magnitude to those that were subsequently measured in Southern California (Eiguren-Fernandez et al., 2008a). We have used the modelled as well as the observed quinone concentrations to make an estimate as to how abundant quinones should be in the particle phase and what their contribution to redox cycling activity would be over a wide range of particle mass loadings.

To predict particulate quinone mass loadings under different mass loadings of organic aerosol, the K_p equation was rearranged to yield $c_p = (K_p/M_p)c_T/(1 + K_p/M_p)$, where c_T is the total quinone mass loading $(c_p + c_g)$ and K_p/M_p is the ratio of the particle-phase mass loading and the gas-phase mass loading of the quinone. Using a quinone concentration of 1 $ng\,m^{-3}$, the particulate mass loading was calculated for 25 °C based on the experimentally determined gas–particle partitioning coefficient of $(7.0 \pm 2.5) \times 10^{-4}\,m^3\,\mu g^{-1}$ for 1,4-naphthoquinone. For 1,2-naphthoquinone, the partitioning coefficient was estimated as $4.4 \times 10^{-3}\,m^3\,\mu g^{-1}$ based on the average of the two estimates discussed previously, with the uncertainty in the range of (1.4–9.9) $\times 10^{-4}\,m^3\,\mu g^{-1}$ based on the upper and lower standard deviations of those estimates. The results of the calculations for a range of organic particle mass loadings approximately 0.1–100 $\mu g\,m^{-3}$ are shown in Fig. 10. DTT activity was calculated based on an average DTT decay rate of 2.1×10^{-3} $pmol\,min^{-1}\,pg^{-1}$ and 5.7×10^{-3} $pmol\,min^{-1}\,pg^{-1}$ for 1,4- and 1,2-naphthoquinone, respectively.

Unsurprisingly, the particulate mass loading of each quinone rises substantially as more organic particles are present for partitioning. As a result, the DTT activity per unit volume of air, which is an important metric for exposure to toxic particles, rises with particle mass loading. The DTT activity normalised to particle mass, however, remains relatively unchanged and actually falls somewhat at high particle mass loadings as the additional mass partitioning to particles begins to diminish. Expected mass-normalised DTT decay rates are anticipated to be on the order of 0.02 $pmol\,min^{-1}\,\mu g^{-1}$ for 1,2-naphthoquinone and 0.0015 $pmol\,min^{-1}\,\mu g^{-1}$ for 1,4-naphthoquinone. As PM in Los Angeles has been measured to decay dithiothreitol at rates greater than 20 $pmol\,min^{-1}\,\mu g^{-1}$ (Ntziachristos et al., 2007), both quinones seem to be unlikely contributors to redox activity of ambient particles in that locale.

This is a simplistic analysis of the partitioning behaviour, assuming equilibrium conditions with bulk partitioning. Measured ambient particulate loadings of 1,4-naphthoquinone (Cho et al., 2004; Eiguren-Fernandez et al., 2008a; Valavanidis et al., 2006) are often in excess of

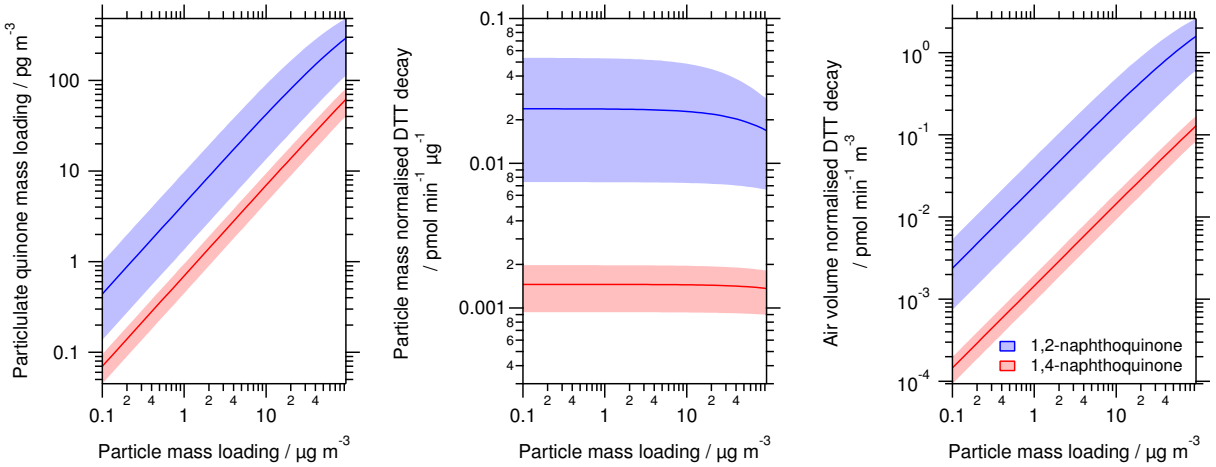

Fig. 10. Calculated quinone particulate mass loadings and mass- and volume-normalised DTT decay rates as a function of organic particle mass loading. Calculations are performed using a total mass concentration of 1 ng m^{-3} of quinone. Shaded areas represent the uncertainties as discussed in the text.

100 pg m^{-3}, which is higher than the range we have estimated based on equilibrium partitioning, perhaps due to non-equilibrium partitioning or partitioning to non-organic aerosol species such as black carbon. We have also not explored how ambient temperature might change the outcome of such an analysis. Naphthoquinone species may become more important under conditions that favour partitioning, namely low temperatures, provided significant naphthalene emissions exist and photoreactivity is sufficiently high. This treatment is beyond the scope of this project but may be important for determining how atmospheric processes may contribute to the toxicity of particles.

Furthermore, there is currently little information on the production rates of the more redox-active and less volatile 1,2-naphthoquinone and 5-hydroxy-1,4-naphthoquinone products for the purpose of atmospheric modelling, and there remains, at minimum, about 70 % of the redox activity with unknown partitioning behaviour that we could not account for based on the three naphthoquinone species measured. The missing activity could arise from highly functionalised products, which are likely to have low vapour pressures and could contribute to redox cycling under ambient particle loading; structural activity relationships predict the vapour pressure of 5-hydroxy-1,4-naphthoquinone to be about an order of magnitude lower than that of 1,4-naphthoquinone (US EPA, 2013). In terms of importance, oxidation of phenanthrene to produce phenanthrenequinone (e.g., Wang et al., 2007; Lee and Lane, 2010), which is of much lower volatility than either 1,2- or 1,4-naphthoquinone and is more highly redox-active, may be a greater source of particle-phase redox-active organic species and has been shown to be an atmospherically relevant species (Eiguren-Fernandez et al., 2008b). Certainly, previous apportioning of DTT activity to chemical species has shown phenanthrenequinone to be a much more substantial contributor to redox activity than 1,2- and 1,4-naphthoquinone (Chung et al., 2006; Charrier and Anastasio, 2012). The influence of naphthalene oxidation on redox activity in relation to other redox active species such as 9,10-phenanthrenequinone, transition metals, black carbon, and humic-like substances – particularly in warmer climates when partitioning favours the gas phase for small naphthoquinones – may ultimately depend on the volatility of the unknown redox-active species generated through its photooxidation.

Acknowledgements. The authors would like to extend thanks to the Mabury group, and in particular Derek Jackson, for the use of their GC-MS and assistance and advice in performing the quinone analysis. Thanks are also extended to the University of Toronto Department of Chemistry for assistance in the design and building of the oxidation chamber. Funding was provided by NSERC and the Canada Foundation for Innovation.

Edited by: M. Ammann

References

Ahmed, S., Kishikawa, N., Ohyama, K., Maki, T., Kurosaki, H., Nakashima, K., and Kuroda, N.: An ultrasensitive and highly selective determination method for quinones by high-performance liquid chromatography with photochemically initiated luminol chemiluminescence, J. Chromatogr. A, 1216, 3977–3984, 2009.

Aiken, A. C., DeCarlo, P. F., and Jimenez, J. L.: Elemental Analysis of Organic Species with Electron Ionization High-Resolution Mass Spectrometry, Anal. Chem., 79, 8350–8358, 2007.

Bunce, N. J., Liu, L., Zhu, J., and Lane, D. A.: Reaction of naphthalene and its derivatives with hydroxyl radicals in the gas phase, Environ. Sci. Technol., 31, 2252–2259, 1997.

Chan, A. W. H., Kautzman, K. E., Chhabra, P. S., Surratt, J. D., Chan, M. N., Crounse, J. D., Kürten, A., Wennberg, P. O., Flagan, R. C., and Seinfeld, J. H.: Secondary organic aerosol formation from photooxidation of naphthalene and alkylnaphthalenes: implications for oxidation of intermediate volatility organic compounds (IVOCs), Atmos. Chem. Phys., 9, 3049–3060, doi:10.5194/acp-9-3049-2009, 2009.

Charrier, J. G. and Anastasio, C.: On dithiothreitol (DTT) as a measure of oxidative potential for ambient particles: evidence for the importance of soluble transition metals, Atmos. Chem. Phys., 12, 9321–9333, doi:10.5194/acp-12-9321-2012, 2012.

Cho, A. K., Di Stefano, E., You, Y., Rodriguez, C. E., Schmitz, D. A., Kumagai, Y., Miguel, A. H., Eiguren-Fernandez, A., Kobayashi, T., Avol, E., and Froines, J. R.: Determination of four quinones in diesel exhaust particles, SRM 1649a, and atmospheric $PM_{2.5}$, Aerosol Sci. Technol., 38, 68–81, 2004.

Cho, A. K., Sioutas, C., Miguel, A. H., Kumagai, Y., Schmitz, D. A., Singh, M., Eiguren-Fernandez, A., and Froines, J. R.: Redox activity of airborne particulate matter at different sites in the Los Angeles Basin, Environ. Res., 99, 40–47, 2005.

Chung, M. Y., Lazaro, R. A., Lim, D., Jackson, J., Lyon, J., Rendulic, D., and Hasson, A. S.: Aerosol-borne quinones and reactive oxygen species generation by particulate matter extracts, Environ. Sci. Technol., 40, 4880–4886, 2006.

DeCarlo, P. F., Kimmel, J. R., Trimborn, A., Northway, M. J., Jayne, J. T., Aiken, A. C., Gonin, M., Fuhrer, K., Horvath, T., Docherty, K. S., Worsnop, D. R., and Jimenez, J. L.: Field-deployable, high-resolution, time-of-flight aerosol mass spectrometer, Anal. Chem., 78, 8281–8289, 2006.

Dellinger, B., Pryor, W. A., Cueto, R., Squadrito, G. L., Hegde, V., and Deutsch, W. A.: Role of free radicals in the toxicity of airborne fine particulate matter, Chem. Res. Toxicol., 14, 1371–1377, 2001.

Eiguren-Fernandez, A., Miguel, A. H., Di Stefano, E., Schmitz, D. A., Cho, A. K., Thurairatnam, S., Avol, E. L., and Froines, J. R.: Atmospheric distribution of gas- and particle-phase quinones in Southern California, Aerosol Sci. Technol., 42, 854–861, 2008a.

Eiguren-Fernandez, A., Miguel, A. H., Lu, R., Purvis, K., Grant, B., Mayo, P., Di Stefano, E., Cho, A. K., and Froines, J.: Atmospheric formation of 9,10-phenanthraquinone in the Los Angeles air basin, Atmos. Environ., 42, 2312–2319, 2008b.

Gant, T. W., Rao, D. N., Mason, R. P., and Cohen, G. M.: Redox cycling and sulphydryl arylation; their relative importance in the mechanism of quinone cytotoxicity to isolated hepatocytes., Chem.-Biol. Interact, 65, 157–173, 1988.

Gurgueira, S. A., Lawrence, J., Coull, B., Murthy, G. G. K., and González-Flecha, B.: Rapid increases in the steady-state concentration of reactive oxygen species in the lungs and heart after particulate air pollution inhalation, Environ. Health Perspect., 110, 749–755, 2002.

Jakober, C. A., Riddle, S. G., Robert, M. A., Destaillats, H., Charles, M. J., Green, P. G., and Kleeman, M. J.: Quinone emissions from gasoline and diesel motor vehicles, Environ. Sci. Technol., 41, 4548–4554, 2007.

Kautzman, K. E., Surratt, J. D., Chan, M. N., Chan, A. W. H., Hersey, S. P., Chhabra, P. S., Dalleska, N. F., Wennberg, P. O., Flagan, R. C., and Seinfeld, J. H.: Chemical composition of gas- and aerosol-phase products from the photooxidation of naphthalene, J. Phys. Chem. A, 114, 913–934, 2010.

Koike, E. and Kobayashi, T.: Chemical and biological oxidative effects of carbon black nanoparticles, Chemosphere, 65, 946–951, 2006.

Kumagai, Y., Koide, S., Taguchi, K., Endo, A., Nakai, Y., Yoshikawa, T., and Shimojo, N.: Oxidation of proximal protein sulfhydryls by phenanthraquinone, a component of diesel exhaust particles, Chem. Res. Toxicol., 15, 483–489, 2002.

Kwamena, N.-O. A., Earp, M. E., Young, C. J., and Abbatt, J. P. D.: Kinetic and product yield study of the heterogeneous gas-surface reaction of anthracene and ozone, J. Phys. Chem. A, 110, 3638–3646, 2006.

Lee, J. and Lane, D. A.: Formation of oxidized products from the reaction of gaseous phenanthrene with the OH radical in a reaction chamber, Atmos. Environ., 44, 2469–2477, 2010.

Lee, J. Y. and Lane, D. A.: Unique products from the reaction of naphthalene with the hydroxyl radical, Atmos. Environ., 43, 4886–4893, 2009.

Li, N., Hao, M., Phalen, R. F., Hinds, W. C., and Nel, A. E.: Particulate air pollutants and asthma. A paradigm for the role of oxidative stress in PM-induced adverse health effects, Clin. Immunol., 109, 250–265, 2003a.

Li, N., Sioutas, C., Cho, A., Schmitz, D., Misra, C., Sempf, J., Wang, M., Oberley, T., Froines, J., and Nel, A.: Ultrafine particulate pollutants induce oxidative stress and mitochondrial damage, Environ. Health Perspect., 111, 455–460, 2003b.

Li, N., Xia, T., and Nel, A. E.: The role of oxidative stress in ambient particulate matter-induced lung diseases and its implications in the toxicity of engineered nanoparticles, Free Radical Biol. Med., 44, 1689–1699, 2008.

Li, Q., Wyatt, A., and Kamens, R. M.: Oxidant generation and toxicity enhancement of aged-diesel exhaust, Atmos. Environ., 43, 1037–1042, 2009.

Lin, P. and Yu, J. Z.: Generation of reactive oxygen species mediated by humic-like substances in atmospheric aerosols, Environ. Sci. Technol., 45, 10362–10368, 2011.

Lu, R., Wu, J., Turco, R. P., Winer, A. M., Atkinson, R., Arey, J., Paulson, S. E., Lurmann, F. W., Miguel, A. H., and Eiguren-Fernandez, A.: Naphthalene distributions and human exposure in Southern California, Atmos. Environ., 39, 489–507, 2005.

McWhinney, R. D., Gao, S. S., Zhou, S., and Abbatt, J. P. D.: Evaluation of the effects of ozone oxidation on redox-cycling activity of two-stroke engine exhaust particles, Environ. Sci. Technol., 45, 2131–2136, 2011.

McWhinney, R. D., Badali, K., Liggio, J., Li, S.-M., and Abbatt, J. P. D.: Filterable redox cycling activity: a comparison between diesel exhaust particles and secondary organic aerosol constituents, Environ. Sci. Technol., 47, 3362–3369, doi:10.1021/es304676x, 2013.

Netto, L. E. S. and Stadtman, E. R.: The iron-catalyzed oxidation of dithiothreitol is a biphasic process: hydrogen peroxide is involved in the initiation of a free radical chain of reactions, Arch. Biochem. Biophys., 333, 233–242, 1996.

NIST Mass Spec Data Centre: "Mass Spectra" in NIST Chemistry WebBook, NIST Standard Reference Database Number 69, National Institute of Standards and Technology, Gaithersburg MD, http://webbook.nist.gov, 2013.

Ntziachristos, L., Froines, J. R., Cho, A. K., and Sioutas, C.: Relationship between redox activity and chemical speciation of

size-fractionated particulate matter, Part. Fibre Toxicol., 4, 5, 2007.

Pan, C.-J. G., Schmitz, D. A., Cho, A. K., Froines, J., and Fukuto, J. M.: Inherent redox properties of diesel exhaust particles: catalysis of the generation of reactive oxygen species by biological reductants, Toxicol. Sci., 81, 225–232, 2004.

Pankow, J. F.: An absorption model of gas/particle partitioning of organic compounds in the atmosphere, Atmos. Environ., 28, 185–188, 1994.

Rattanavaraha, W., Rosen, E., Zhang, H., Li, Q., Pantong, K., and Kamens, R. M.: The reactive oxidant potential of different types of aged atmospheric particles: An outdoor chamber study, Atmos. Environ., 45, 3848–3855, 2011.

Roginsky, V. A., Barsukova, T. K., and Stegmann, H. B.: Kinetics of redox interaction between substituted quinones and ascorbate under aerobic conditions, Chem.-Biol. Interact, 121, 177–197, 1999.

Sasaki, J., Aschmann, S. M., Kwok, E. S. C., Atkinson, R., and Arey, J.: Products of the gas-phase OH and NO_3 radical-initiated reactions of naphthalene, Environ. Sci. Technol., 31, 3173–3179, 1997.

Shakya, K. M. and Griffin, R. J.: Secondary organic aerosol from photooxidation of polycyclic aromatic hydrocarbons, Environ. Sci. Technol., 44, 8134–8139, 2010.

Shinyashiki, M., Eiguren-Fernandez, A., Schmitz, D. A., Di Stefano, E., Li, N., Linak, W. P., Cho, S.-H., Froines, J. R., and Cho, A. K.: Electrophilic and redox properties of diesel exhaust particles, Environ. Res., 109, 239–244, 2009.

Shiraiwa, M., Ammann, M., Koop, T., and Pöschl, U.: Gas uptake and chemical aging of semisolid organic aerosol particles, P. Natl. Acad. Sci., 108, 11003–11008, 2011.

Sousa, E. T., da Silva, M. M., de Andrade, S. J., Cardoso, M. P., Silva, L. A., and de Andrade, J. B.: Evaluation of thermal stability of quinones by thermal analysis techniques, Thermochim. Acta, 529, 1–5, 2012.

Squadrito, G. L., Cueto, R., Dellinger, B., and Pryor, W. A.: Quinoid redox cycling as a mechanism for sustained free radical generation by inhaled airborne particulate matter, Free Radical Biol. Med., 31, 1132–1138, 2001.

Tsapakis, M. and Stephanou, E. G.: Diurnal cycle of PAHs, nitro-PAHs, and oxy-PAHs in a high oxidation capacity marine background atmosphere, Environ. Sci. Technol., 41, 8011–8017, 2007.

US EPA: Estimations Programs Interface Suite™ for Microsoft™ Windows, v 4.11., United States Environmental Protection Agency, Washington DC, 2013.

Valavanidis, A., Fiotakis, K., Vlahogianni, T., Papadimitriou, V., and Pantikaki, V.: Determination of selective quinones and quinoid radicals in airborne particulate matter and vehicular exhaust particles, Environ. Chem., 3, 118–123, 2006.

Verma, V., Ning, Z., Cho, A. K., Schauer, J. J., Shafer, M. M., and Sioutas, C.: Redox activity of urban quasi-ultrafine particles from primary and secondary sources, Atmos. Environ., 43, 6360–6368, 2009.

Verma, V., Rico-Martinez, R., Kotra, N., King, L., Liu, J., Snell, T. W., and Weber, R. J.: Contribution of water-soluble and insoluble components and their hydrophobic/hydrophilic subfractions to the reactive oxygen species-generating potential of fine ambient aerosols, Environ. Sci. Technol., 46, 11384–11392, 2012.

Wang, L., Atkinson, R., and Arey, J.: Formation of 9,10-phenanthrenequinone by atmospheric gas-phase reactions of phenanthrene, Atmos. Environ., 41, 2025–2035, 2007.

Wardman, P.: Reduction potentials of one-electron couples involving free-radicals in aqueous-solution, J. Phys. Chem. Ref. Data, 18, 1637–1755, 1989.